Cosmic Ray Anisotropy with 11 Years of IceCube Data

The IceCube Collaboration

(a complete list of authors can be found at the end of the proceedings)

E-mail: mcnally_ft@mercer.edu

The IceCube Observatory provides our highest-statistics picture of the cosmic-ray arrival directions in the Southern Hemisphere, with over 700 billion cosmic-ray-induced muon events collected between May 2011 and May 2022. Using the larger data volume, we find an improved significance of the PeV cosmic ray anisotropy down to scales of $6°$. In addition, we observe a variation in the angular power spectrum as a function of energy, hinting at a relative decrease in large-scale features above 100 TeV. The data-taking period covers a complete solar cycle, providing new insight into the time variability of the signal. We present preliminary results using this up-to-date event sample.

Corresponding authors: Frank McNally[1*], Rasha Abbasi[2], Paolo Desiati[3], Juan Carlos Díaz Vélez[3], Christina Cochling[1], Katherine Gruchot[2], William Hayes[2], Andrew Moy[2], Emily Schmidt[1], and Andrew Thorpe[1]

[1] *Mercer University, U.S.A.*

[2] *Loyola University Chicago, U.S.A.*

[3] *University of Wisconsin - Madison, U.S.A.*

[*] Presenter

1. Introduction

One of the goals of astrophysical observations is to identify the sources of cosmic rays and the mechanism by which they are accelerated and injected into the interstellar medium. The cosmic ray particles observed on Earth carry the general properties of the sources from which they originated and the medium traversed in their journey. The study of cosmic ray transport is a key to understanding their astrophysical origin. Most investigations rely on the information derived from energy spectrum and mass composition measurements. However, measuring their arrival direction offers a method to study the cosmic ray pitch angle distribution in the interstellar medium, which provides a direct probe of interstellar diffusion properties [1]. Several theoretical models predict an anisotropy in the cosmic ray arrival directions that results from the distribution of sources in the Milky Way and diffusive propagation of these particles [2–11].

Over the last two decades, large and modern ground-based experiments have provided high-volume data that facilitate state-of-the-art analyses of cosmic ray anisotropy in the TeV-PeV energy range (see [12–18] and references therein). The observed anisotropy (up to the order of 10^{-3} in relative intensity) possesses a complex structure manifesting at different angular scales. It also appears to evolve with energy as well. New generation experiments currently under design (e.g., SWGO [19, 20] and IceCube-Gen2 [21]) will further enhance the scientific reach, in addition to making it possible to provide additional full-sky coverage for unbiased anisotropy observations.

This work presents the up-to-date cosmic ray anisotropy results observed by the IceCube Observatory using about 700 billion events collected from 2011 to 2022. IceCube is an astroparticle observatory at the geographic South Pole, consisting of a cubic kilometer of instrumented volume over a kilometer under the ice surface, sensitive to cosmic rays via the muonic component of air showers [22]. The observation shows the evolution of the arrival direction distribution from 10 TeV to 530 TeV median energy, with high statistical significance.

2. Data Analysis

The methods used in this analysis are largely consistent with previous anisotropy studies in IceCube [12–14, 16, 23]. We incorporated improvements in the cosmic-ray shower physics, the experiment's response in our Monte Carlo simulation, and systematics since the last major publication, as presented in Ref. [24]. The most significant change lies in the increased statistics (over a factor of two compared to the results in Ref. [16]), allowing for more detailed energetic studies and spanning a full solar cycle.

To analyze cosmic-ray anisotropy, we first need to build a reference map representing the detector's sensitivity to an isotropic cosmic-ray flux. For this, we use a time scrambling method [13]. The data map contains the directions of events in sidereal coordinates (RA, Dec) calculated from their local coordinates (θ, ϕ) and arrival time t. To build the reference map, each event in the dataset is assigned a random time sampled from the time distribution of all events over a time window Δt. This approach maintains both the local arrival direction distribution and the temporal distribution of events while scrambling their sidereal coordinates. For every real event in the data, we generate 20 time-scrambled events in order to reduce statistical fluctuations. The IceCube detector rate is very stable over a period of 24 h, which means we can choose $\Delta t = 24$ h.

Once we have constructed a reference map, we can compute the relative intensity for each pixel in the map by

$$\frac{\delta I_i}{I_i} = \frac{N_i - \langle N_i \rangle}{\langle N_i \rangle} \,,\tag{1}$$

where N_i and $\langle N_i \rangle$ are the number of events at the ith pixel of the data map and the reference map, respectively. The statistical significance of any deviation from the reference level can be calculated using the Li & Ma method [25]. This method takes into account statistical fluctuations in data and reference counts. We apply "top-hat" smoothing to the data and reference maps in order to increase the sensitivity to regions with excess at different angular sizes by adding all counts within a given angular radius of each pixel.

The energy reconstruction is performed using a simple lookup table. Simulated events are weighted to a Gaisser H3a composition model [26] and binned based on the number of digital optical modules (DOMs) triggered (N_{channel}) and the reconstructed arrival direction of the cosmic ray primary (θ_{reco}). Both of these parameters correlate strongly with the energy of observed events — more energetic showers trigger more DOMs on average, and showers with larger zenith angles must pass through more of the atmosphere, filtering out lower-energy events. Each bin is then assigned its median energy value and we smooth the table to avoid statistical artifacts at the highest energies where simulation is limited (Fig. 1). Using this table, each event is assigned an energy bin based on its N_{channel} and θ_{reco} values.

The reconstructed energy bins have true energy distributions that overlap significantly, but we can still use them to study changes in

Figure 1: Median cosmic-ray primary energy as a function of reconstructed shower direction ($\cos\theta$) and number of DOMs triggered ($\log_{10} N$). This table is the result of a 2D-histogram populated using simulated events, then smoothed with splines to avoid low-statistics artifacts at the highest energies.

the observed anisotropy as a function of energy. Previous studies show wide regions of excess and deficit (right ascensions of 30-120° and 150-250°, respectively) at low energies, replaced by a wide, dominant deficit centered at a right ascension of about 80° [16, 24]. Despite reduced statistics, the high-energy deficit is sufficiently strong to make a visible impact on the large-scale structure map, previously reported using all observed events. For this reason, we now show the large- and small-scale structure visible in the Southern Hemisphere using only the lowest energy bin. This approach should help disentangle the separate low- and high-energy signals. A high-energy map is also shown, consisting of the three highest energy bins in our analysis (i.e., events with $\log_{10}(E/\text{GeV}) > 5.5$). The true energy distributions have median energies of 13 and 530 TeV, respectively, with a 25% overlap.
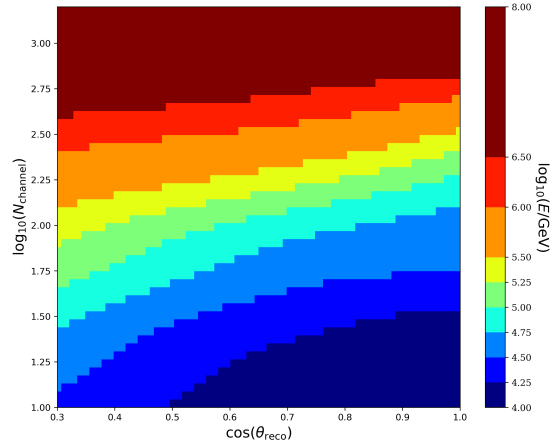
3. Results

Figure 2 shows the large- and small-scale structure for the lowest reconstructed energy bin. The large-scale structure map is largely equivalent to the energy-binned maps shown in previous analyses [16, 24], with large regions of excess and deficit observed at high significance. The map of small-scale structure is new, having previously only been shown for all events. In previous studies, there was a deficit in the small-scale map located between right ascensions of $60 - 90°$. No significant structure is present in the low-energy small-scale structure at that location, indicating that previous observations featured signal contamination from high-energy events.
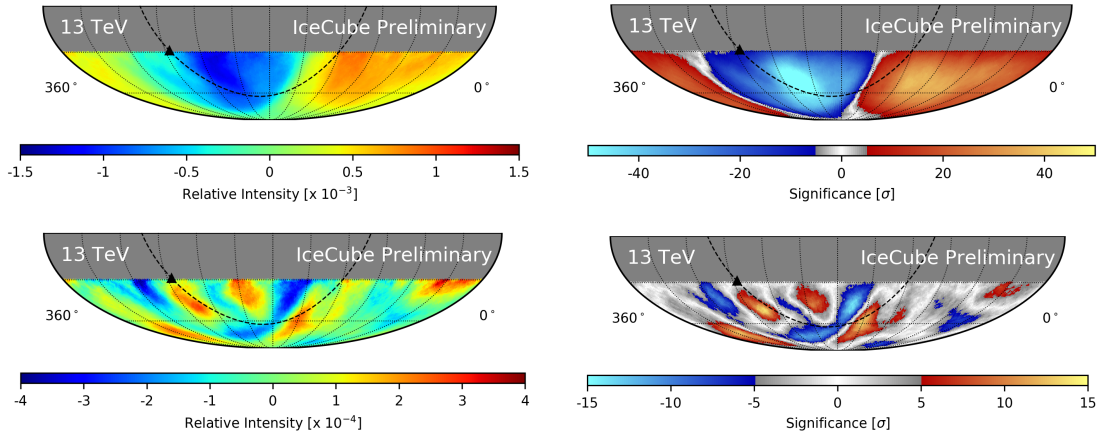

Figure 2: Relative intensity (*left*) and significance (*right*) for events with $\log_{10}(E_{\text{reco}}/\text{GeV}) < 4.25$. Maps are in equatorial coordinates and have a top-hat smoothing radius of $5°$. The large-scale structure (*top*) is the result of considering all events. The small-scale structure (*bottom*) represents the residual signal after subtracting off the best-fit dipole and quadrupole components. Pixels below a 5σ threshold in the significance map are shown in grayscale.

At higher energies, the only significant feature continues to be the deficit located at a right ascension of about $80°$, as shown in Fig. 3. To account for the reduced statistics at these energies, we used a larger smoothing radius consistent with previous energy analyses ($20°$), as opposed to the $5°$ radius commonly used in large- and small-scale structure studies. The map of the small-scale structure is omitted as, even with this larger smoothing radius, no significant structure is observed.
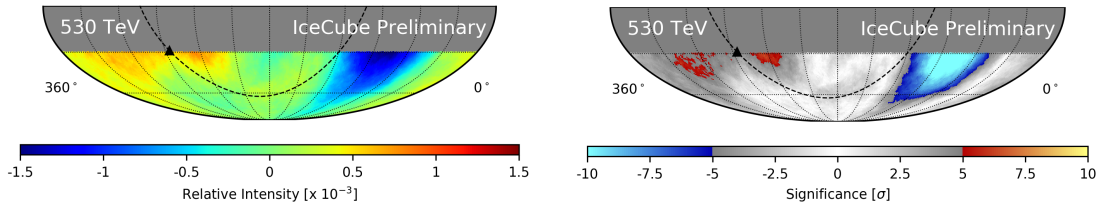

Figure 3: Relative intensity (*left*) and significance (*right*) maps for all events with $\log_{10}(E_{\text{reco}}/\text{GeV}) > 5.5$. Maps are in equatorial coordinates and have a top-hat smoothing radius of $20°$. Pixels below a 5σ threshold are shown in grayscale.

The increased statistics of the 11-year dataset allow for IceCube's first look at the angular power spectrum of the cosmic ray anisotropy as a function of energy. Figure 4 shows the power spectra for each energy bin, excepting the highest-energy one where we lack sufficient statistics. The shaded noise bands represent 1, 2, and 3σ containment for power spectra produced in response to an isotropic sky, simulated by varying background maps within Poisson uncertainties. The increasing power of the noise floor with energy is the result of decreasing statistics. It is important to note that these plots display the *observed* power spectra — IceCube's partial sky coverage results in correlation between multipoles, producing a ringing effect. This effect is avoidable only through collaborative full-sky analyses with other detectors [27].

An alternative method of visualizing the change in the angular power spectra over energy is to plot the behavior of a single multipole. Figure 5 shows the phase and amplitude of the dipole component as a function of energy, as compared to the results from other experiments. The calculation methods for this plot are slightly different; following the procedure used in Ref. [16], we instead use a harmonic fit (up to $\ell = 3$) on a one-dimensional projection of the relative intensity as a function of right ascension. The resultant dipole component displays a transition in phase and amplitude occurring near 100 TeV — consistent with previous work in IceCube and results from other experiments.

In order to look for time-dependent variation in the anisotropy, we use the same one-dimensional projection as when finding the phase and amplitude of a best-fit dipole. Figure 6 shows the relative intensity for bins in right ascension, with each data series representing a different calendar year. Use of calendar years greatly reduces the systematic uncertainty of solar influences on the sidereal signal as seen in the anti-sidereal frame, making statistical and systematic uncertainties of similar magnitude [24]. Combined with the extended observation period, the reduced systematic uncertainties hint at the potential for time-dependent behavior in some bins, where the variations are greater than expected systematic variations about the 11-year average values shown in gray. A study dedicated to determining the significance of this effect is planned.

4. Conclusion

We have analyzed over 700 billion cosmic-ray-induced muon events collected by the IceCube Neutrino Observatory between May 2011 and May 2022 to study the arrival direction distribution of cosmic rays in the TeV-PeV energy range. The increased event volume by a factor of two since our last report [16] made it possible to improve the significance of the large- and small-scale structures of the cosmic ray anisotropy up to PeV energies and down to scales of 6°.

The latest study includes several improvements to previous IceCube analyses of the observed anisotropy in cosmic ray arrival direction. The observed angular structures and power spectrum are consistent with previous measurements, but we can now report significant features in our highest-energy map. In addition, we observe a variation in the angular power spectrum as a function of energy, hinting at a relative decrease in large-scale features above 100 TeV.

In addition to greater statistics, the use of single detector geometry enables the study of data by calendar year as opposed to detector year and thus reduces systematic uncertainties in the sidereal anisotropy that arise from interference with the solar frame. Additional improvements in our simulations and a larger Monte Carlo sample result in better energy reconstructions.
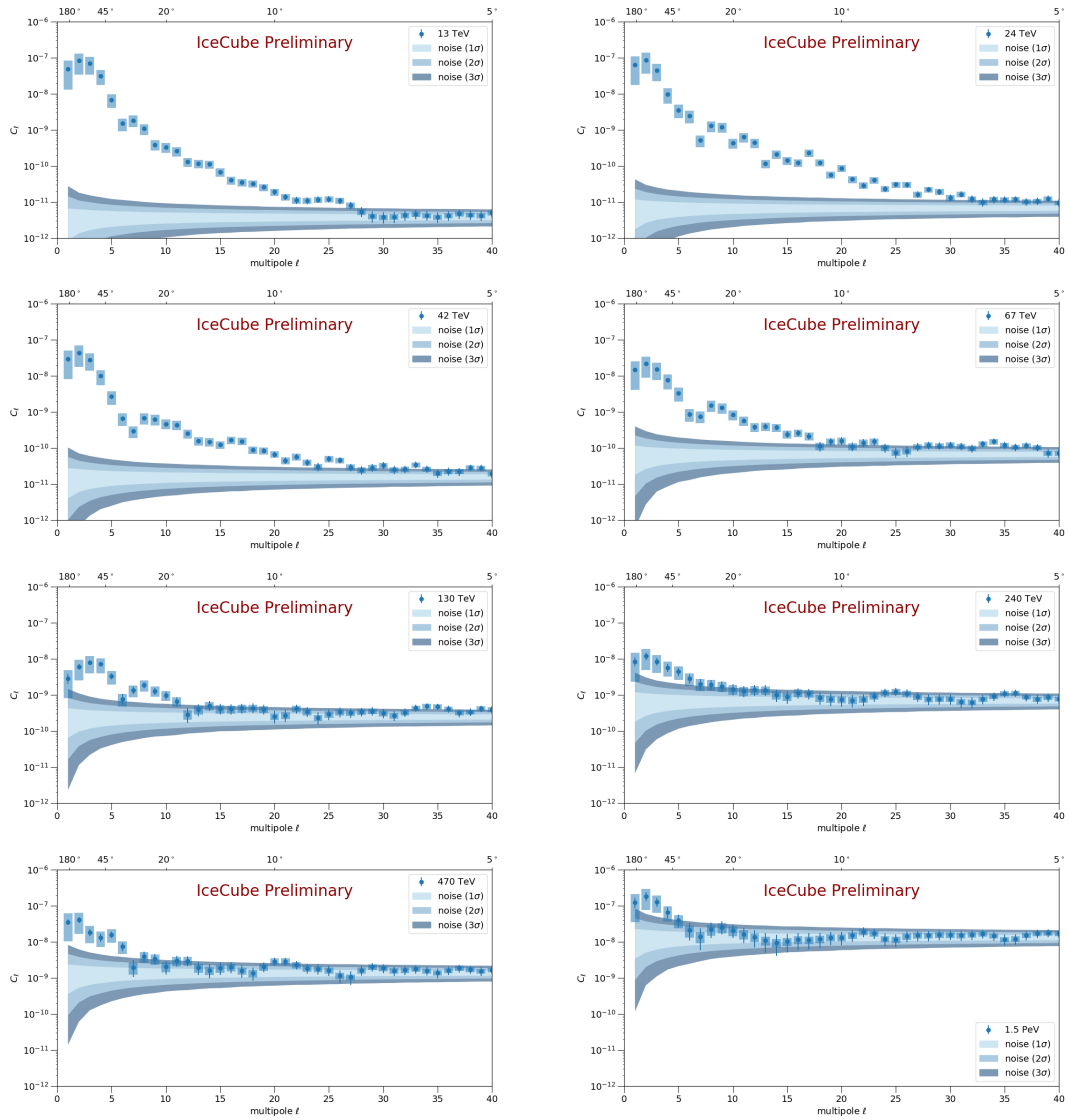
Figure 4: Angular power spectra for the energy bins shown in Fig. 1. Systematic uncertainties (*shaded boxes*) represent a standard deviation of power spectra calculated using identical input C_ℓ values with random orientations. Statistical uncertainties (*error bars*) are calculated by fluctuating pixel counts within Poisson uncertainties. The large shaded bands represent the reconstructed power from an isotropic sky. The highest energy bin ($\log_{10}(E_{\text{reco}}/\text{GeV}) > 6.5$) is omitted, as its power lies within the isotropic bands at all multipoles.

References

[1] P. Desiati, J. C. D. Vélez, N. Pogorelov, and M. Zhang, "Snowmass 2021 loi: Determination of cosmic ray properties in the local interstellar medium with all-sky anisotropy observations," 2020.

[2] A. D. Erlykin and A. W. Wolfendale *Astropart. Phys.* **25** (Apr., 2006) 183–194.

[3] P. Blasi and E. Amato *JCAP* **1** (2012) 11.

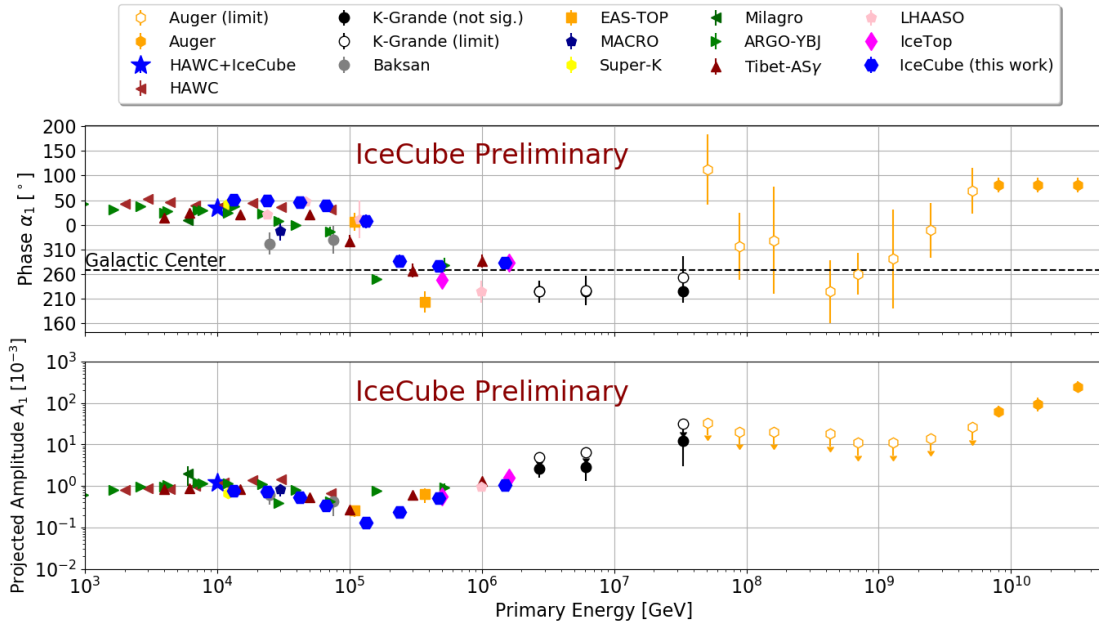[4] V. Ptuskin *Astropart. Phys.* **39** (2012) 44–51.

Figure 5: Phase (*top*) and amplitude (*bottom*) of the best-fit dipole component as a function of reconstructed energy, shown in comparison to results from other experiments. The phase and amplitude are calculated using a harmonic fit up to $\ell = 3$ for a one-dimensional projection of the relative intensity along right ascension. Results shown are from [15, 18, 27–38].

[5] M. Pohl and D. Eichler *Astrophys. J.* **766** (2013) 4.

[6] L. G. Sveshnikova *et al. Astropart. Phys.* **50** (2013) 33–46.

[7] R. Kumar and D. Eichler *Astrophys. J.* **785** (2014) 129.

[8] P. Mertsch and S. Funk *Phys. Rev. Lett.* **114** (2015) 021101.

[9] M. Ahlers *Phys. Rev. Lett.* **112** no. 2, (2014) 021101.

[10] M. Ahlers and P. Mertsch *Astrophys. J.* **815** no. 1, (2015) L2.

[11] M. Ahlers *Phys. Rev. Lett.* **117** no. 15, (2016) 151103.

[12] **IceCube** Collaboration, R. Abbasi *et al. Astrophys. J.* **718** (2010) L194.

[13] **IceCube** Collaboration, R. Abbasi *et al. Astrophys. J.* **740** (2011) 16.

[14] **IceCube** Collaboration, R. Abbasi *et al. Astrophys. J.* **746** (2012) 33.

[15] **IceCube** Collaboration, M. Aartsen *et al. Astrophys. J.* **765** (2013) 55.

[16] **IceCube** Collaboration, M. G. Aartsen *et al. Astrophys. J.* **826** (2016) 220.

[17] **IceCube, HAWC** Collaboration, J. C. Díaz-Vélez *et al. PoS* **ICRC2017** (2017) .

[18] **LHAASO** Collaboration, W. Gao *et al. PoS* **ICRC2021** (2021) 351.

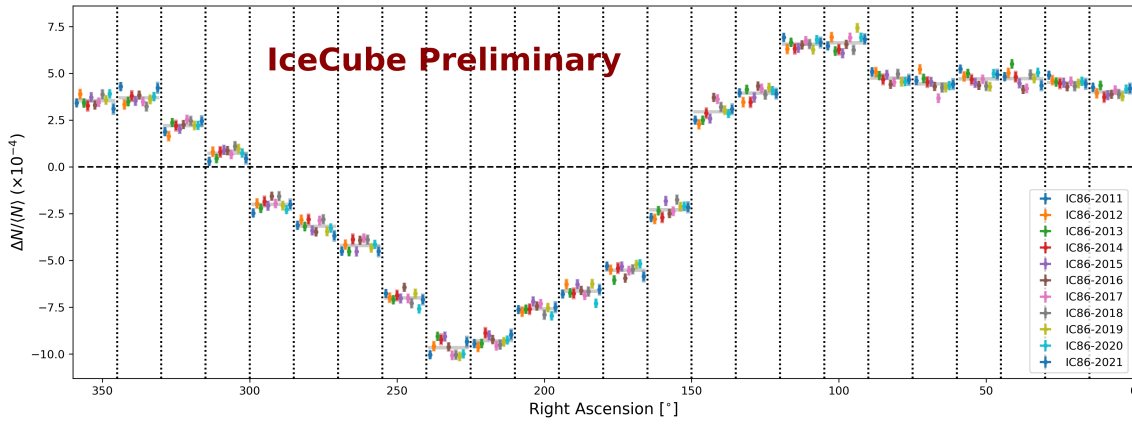[19] A. Albert *et al.* arXiv:1902.08429.

Figure 6: Comparison of relative intensity as a function of time, shown as a one-dimensional projection binned in right ascension. Each series represents one calendar year, beginning and ending in May. Both statistical (*error bars*) and systematic (*shaded boxes*) uncertainties are included, the latter being calculated from the root-mean-square of the anti-sidereal distribution for the corresponding year. The narrow gray band in each bin indicates the relative intensity and uncertainty for the combined dataset.

[20] N. Fraija *et al. Astro2020: Decadal Survey on Astronomy and Astrophysics* **2020** (2019) 459.

[21] **IceCube** Collaboration, M. G. Aartsen *et al. J. Phys. G* **48** no. 6, (2021) 060501.

[22] **IceCube** Collaboration, R. Abbasi *et al. Nucl. Instrum. Meth.* **A601** (2009) 294–316.

[23] **IceCube** Collaboration, J. Bourbeau, P. Desiati, J. C. Díaz Vélez, and S. Westerhoff *PoS* **ICRC2017** (2017) 474.

[24] **IceCube** Collaboration, R. Abbasi *et al. PoS* **ICRC2021** (2021) 320.

[25] T. P. Li and Y. Q. Ma *Astrophys. J.* **272** (1983) 317–324.

[26] T. K. Gaisser *Astropart. Phys.* **35** (2012) 801–806.

[27] **HAWC** Collaboration, A. U. Abeysekara *et al. Astrophys. J.* **871** no. 1, (2019) 96.

[28] **HAWC** Collaboration, A. U. Abeysekara *et al. Astrophys. J.* **865** no. 1, (2018) 57.

[29] **KASCADE-Grande** Collaboration, W. D. Apel *et al. Astrophys. J.* **870** no. 2, (2019) 91.

[30] V. V. Alekseenko *et al. Nucl Phys B Proc Suppl.* **196** (2009) 179–182.

[31] **EAS-TOP** Collaboration, M. Aglietta *et al. Astrophys. J.* **692** (2009) L130–L133.

[32] **MACRO** Collaboration, M. Ambrosio and et al. *Phys. Rev. D* **67** no. 4, (2003) 042002.

[33] **Super-Kamiokande** Collaboration, G. Guillian *et al. Phys. Rev. D* **75** (2007) 062003.

[34] **Milagro** Collaboration, A. A. Abdo *et al. Astrophys. J.* **698** (2009) 2121–2130.

[35] **ARGO-YBJ** Collaboration, B. Bartoli *et al. Astrophys. J.* **809** no. 1, (2015) 90.

[36] **ARGO-YBJ** Collaboration, B. Bartoli *et al. Astrophys. J.* **861** (2018) 93.

[37] **Tibet AS**γ Collaboration, M. Amenomori *et al. Astrophys. J.l* **626** no. 1, (2005) L29.

[38] **Pierre Auger** Collaboration, A. Aab *et al. Astrophys. J.* **891** no. 2, (2020) 142.

Full Author List: IceCube Collaboration

R. Abbasi[17], M. Ackermann[63], J. Adams[18], S. K. Agarwalla[40, 64], J. A. Aguilar[12], M. Ahlers[22], J.M. Alameddine[23], N. M. Amin[44], K. Andeen[42], G. Anton[26], C. Argüelles[14], Y. Ashida[53], S. Athanasiadou[63], S. N. Axani[44], X. Bai[50], A. Balagopal V.[40], M. Baricevic[40], S. W. Barwick[30], V. Basu[40], R. Bay[8], J. J. Beatty[20, 21], J. Becker Tjus[11, 65], J. Beise[61], C. Bellenghi[27], C. Benning[1], S. BenZvi[52], D. Berley[19], E. Bernardini[48], D. Z. Besson[36], E. Blaufuss[19], S. Blot[63], F. Bontempo[31], J. Y. Book[14], C. Boscolo Meneguolo[48], S. Böser[41], O. Botner[61], J. Böttcher[1], E. Bourbeau[22], J. Braun[40], B. Brinson[6], J. Brostean-Kaiser[63], R. T. Burley[2], R. S. Busse[43], D. Butterfield[40], M. A. Campana[49], K. Carloni[14], E. G. Carnie-Bronca[2], S. Chattopadhyay[40, 64], N. Chau[12], C. Chen[6], Z. Chen[55], D. Chirkin[40], S. Choi[56], B. A. Clark[19], L. Classen[43], C. Cochling[38], A. Coleman[61], G. H. Collin[15], A. Connolly[20, 21], J. M. Conrad[15], P. Coppin[13], P. Correa[13], D. F. Cowen[59, 60], P. Dave[6], C. De Clercq[13], J. J. DeLaunay[58], D. Delgado[14], S. Deng[1], K. Deoskar[54], A. Desai[40], P. Desiati[40], K. D. de Vries[13], G. de Wasseige[37], T. DeYoung[24], A. Diaz[15], J. C. Díaz-Vélez[40], M. Dittmer[43], A. Domi[26], H. Dujmovic[40], M. A. DuVernois[40], T. Ehrhardt[41], P. Eller[27], E. Ellinger[62], S. El Mentawi[1], D. Elsässer[23], R. Engel[31, 32], H. Erpenbeck[40], J. Evans[19], P. A. Evenson[44], K. L. Fan[19], K. Fang[40], K. Farrag[16], A. R. Fazely[7], A. Fedynitch[57], N. Feigl[10], S. Fiedlschuster[26], C. Finley[54], L. Fischer[63], D. Fox[59], A. Franckowiak[11], A. Fritz[41], P. Fürst[1], J. Gallagher[39], E. Ganster[1], A. Garcia[14], L. Gerhardt[9], A. Ghadimi[58], C. Glaser[61], T. Glauch[27], T. Glüsenkamp[26, 61], N. Goehlke[32], J. G. Gonzalez[44], S. Goswami[58], D. Grant[24], S. J. Gray[19], O. Gries[1], S. Griffin[40], S. Griswold[52], K. M. Groth[22], K. Gruchot[17], C. Günther[1], P. Gutjahr[23], C. Haack[26], A. Hallgren[61], R. Halliday[24], L. Halve[1], F. Halzen[40], H. Hamdaoui[55], M. Ha Minh[27], K. Hanson[40], J. Hardin[15], A. A. Harnisch[24], P. Hatch[33], A. Haungs[31], W. Hayes[17], K. Helbing[62], J. Hellrung[11], F. Henningsen[27], L. Heuermann[1], N. Heyer[61], S. Hickford[62], A. Hidvegi[54], C. Hill[16], G. C. Hill[2], K. D. Hoffman[19], S. Hori[40], K. Hoshina[40, 66], W. Hou[31], T. Huber[31], K. Hultqvist[54], M. Hünnefeld[23], R. Hussain[40], K. Hymon[23], S. In[56], A. Ishihara[16], M. Jacquart[40], O. Janik[1], M. Jansson[54], G. S. Japaridze[5], M. Jeong[56], M. Jin[14], B. J. P. Jones[4], D. Kang[31], W. Kang[56], X. Kang[49], A. Kappes[43], D. Kappesser[41], L. Kardum[23], T. Karg[63], M. Karl[27], A. Karle[40], U. Katz[26], M. Kauer[40], J. L. Kelley[40], A. Khatee Zathul[40], A. Kheirandish[34, 35], J. Kiryluk[55], S. R. Klein[8, 9], A. Kochocki[24], R. Koirala[44], H. Kolanoski[10], T. Kontrimas[27], L. Köpke[41], C. Kopper[26], D. J. Koskinen[22], P. Koundal[31], M. Kovacevich[49], M. Kowalski[10, 63], T. Kozynets[22], J. Krishnamoorthi[40, 64], K. Kruiswijk[37], E. Krupczak[24], A. Kumar[63], E. Kun[11], N. Kurahashi[49], N. Lad[63], C. Lagunas Gualda[63], M. Lamoureux[37], M. J. Larson[19], S. Latseva[1], F. Lauber[62], J. P. Lazar[14, 40], J. W. Lee[56], K. Leonard DeHolton[60], A. Leszczyńska[44], M. Lincetto[11], Q. R. Liu[40], M. Liubarska[25], E. Lohfink[41], C. Love[49], C. J. Lozano Mariscal[43], L. Lu[40], F. Lucarelli[28], W. Luszczak[20, 21], Y. Lyu[8, 9], J. Madsen[40], K. B. M. Mahn[24], Y. Makino[40], E. Manao[27], S. Mancina[40, 48], W. Marie Sainte[40], I. C. Mariş[12], S. Marka[46], Z. Marka[46], M. Marsee[58], I. Martinez-Soler[14], R. Maruyama[45], F. Mayhew[24], T. McElroy[25], F. McNally[38], J. V. Mead[22], K. Meagher[40], S. Mechbal[63], A. Medina[21], M. Meier[16], Y. Merckx[13], L. Merten[11], J. Micallef[24], J. Mitchell[7], T. Montaruli[28], R. W. Moore[25], Y. Morii[16], R. Morse[40], M. Moulai[40], A. Moy[17], T. Mukherjee[31], R. Naab[63], R. Nagai[16], M. Nakos[40], U. Naumann[62], J. Necker[63], A. Negi[4], M. Neumann[43], H. Niederhausen[24], M. U. Nisa[24], A. Noell[1], A. Novikov[44], S. C. Nowicki[24], A. Obertacke Pollmann[16], V. O'Dell[40], M. Oehler[31], B. Oeyen[29], A. Olivas[19], R. Ørsøe[27], J. Osborn[40], E. O'Sullivan[61], H. Pandya[44], N. Park[33], G. K. Parker[4], E. N. Paudel[44], L. Paul[42, 50], C. Pérez de los Heros[61], J. Peterson[40], S. Philippen[1], A. Pizzuto[40], M. Plum[50], A. Pontén[61], Y. Popovych[41], M. Prado Rodriguez[40], B. Pries[24], R. Procter-Murphy[19], G. T. Przybylski[9], C. Raab[37], J. Rack-Helleis[41], K. Rawlins[3], Z. Rechav[40], A. Rehman[44], P. Reichherzer[11], G. Renzi[12], E. Resconi[27], S. Reusch[63], W. Rhode[23], B. Riedel[40], A. Rifaie[1], E. J. Roberts[2], S. Robertson[8, 9], S. Rodan[56], G. Roellinghoff[56], M. Rongen[26], C. Rott[53, 56], T. Ruhe[23], L. Ruohan[27], D. Ryckbosch[29], I. Safa[14, 40], J. Saffer[32], D. Salazar-Gallegos[24], P. Sampathkumar[31], S. E. Sanchez Herrera[24], A. Sandrock[62], M. Santander[58], S. Sarkar[25], S. Sarkar[47], J. Savelberg[1], P. Savina[40], M. Schaufel[1], H. Schieler[31], S. Schindler[26], L. Schlickmann[1], B. Schlüter[43], F. Schlüter[12], N. Schmeisser[62], E. Schmidt[38], T. Schmidt[19], J. Schneider[26], F. G. Schröder[31, 44], L. Schumacher[26], G. Schwefer[1], S. Sclafani[19], D. Seckel[44], M. Seikh[36], S. Seunarine[51], R. Shah[49], A. Sharma[61], S. Shefali[32], N. Shimizu[16], M. Silva[40], B. Skrzypek[14], B. Smithers[4], R. Snihur[40], J. Soedingrekso[23], A. Søgaard[22], D. Soldin[32], P. Soldin[1], G. Sommani[11], C. Spannfellner[27], G. M. Spiczak[51], C. Spiering[63], M. Stamatikos[21], T. Stanev[44], T. Stezelberger[9], T. Stürwald[62], T. Stuttard[22], G. W. Sullivan[19], I. Taboada[6], S. Ter-Antonyan[7], M. Thiesmeyer[1], W. G. Thompson[14], A. Thorpe[38], J. Thwaites[40], S. Tilav[44], K. Tollefson[24], C. Tönnis[56], S. Toscano[12], D. Tosi[40], A. Trettin[63], C. F. Tung[6], R. Turcotte[31], J. P. Twagirayezu[24], B. Ty[40], M. A. Unland Elorrieta[43], A. K. Upadhyay[40, 64], K. Upshaw[7], N. Valtonen-Mattila[61], J. Vandenbroucke[40], N. van Eijndhoven[13], D. Vannerom[15], J. van Santen[63], J. Vara[43], J. Veitch-Michaelis[40], M. Venugopal[31], M. Vereecken[37], S. Verpoest[44], D. Veske[46], A. Vijai[19], C. Walck[54], C. Weaver[24], P. Weigel[15], A. Weindl[31], J. Weldert[60], C. Wendt[40], J. Werthebach[23], M. Weyrauch[31], N. Whitehorn[24], C. H. Wiebusch[1], N. Willey[24], D. R. Williams[58], L. Witthaus[23], A. Wolf[1], M. Wolf[27], G. Wrede[26], X. W. Xu[7], J. P. Yanez[25], E. Yildizci[40], S. Yoshida[16], R. Young[36], F. Yu[14], S. Yu[24], T. Yuan[40], Z. Zhang[55], P. Zhelnin[14], M. Zimmerman[40]

[1] III. Physikalisches Institut, RWTH Aachen University, D-52056 Aachen, Germany

[2] Department of Physics, University of Adelaide, Adelaide, 5005, Australia

[3] Dept. of Physics and Astronomy, University of Alaska Anchorage, 3211 Providence Dr., Anchorage, AK 99508, USA

[4] Dept. of Physics, University of Texas at Arlington, 502 Yates St., Science Hall Rm 108, Box 19059, Arlington, TX 76019, USA

[5] CTSPS, Clark-Atlanta University, Atlanta, GA 30314, USA

[6] School of Physics and Center for Relativistic Astrophysics, Georgia Institute of Technology, Atlanta, GA 30332, USA

[7] Dept. of Physics, Southern University, Baton Rouge, LA 70813, USA

[8] Dept. of Physics, University of California, Berkeley, CA 94720, USA

[9] Lawrence Berkeley National Laboratory, Berkeley, CA 94720, USA

[10] Institut für Physik, Humboldt-Universität zu Berlin, D-12489 Berlin, Germany

[11] Fakultät für Physik & Astronomie, Ruhr-Universität Bochum, D-44780 Bochum, Germany

[12] Université Libre de Bruxelles, Science Faculty CP230, B-1050 Brussels, Belgium

[13] Vrije Universiteit Brussel (VUB), Dienst ELEM, B-1050 Brussels, Belgium

[14] Department of Physics and Laboratory for Particle Physics and Cosmology, Harvard University, Cambridge, MA 02138, USA

[15] Dept. of Physics, Massachusetts Institute of Technology, Cambridge, MA 02139, USA

[16] Dept. of Physics and The International Center for Hadron Astrophysics, Chiba University, Chiba 263-8522, Japan

[17] Department of Physics, Loyola University Chicago, Chicago, IL 60660, USA

[18] Dept. of Physics and Astronomy, University of Canterbury, Private Bag 4800, Christchurch, New Zealand

[19] Dept. of Physics, University of Maryland, College Park, MD 20742, USA

[20] Dept. of Astronomy, Ohio State University, Columbus, OH 43210, USA

[21] Dept. of Physics and Center for Cosmology and Astro-Particle Physics, Ohio State University, Columbus, OH 43210, USA

[22] Niels Bohr Institute, University of Copenhagen, DK-2100 Copenhagen, Denmark

[23] Dept. of Physics, TU Dortmund University, D-44221 Dortmund, Germany

[24] Dept. of Physics and Astronomy, Michigan State University, East Lansing, MI 48824, USA

[25] Dept. of Physics, University of Alberta, Edmonton, Alberta, Canada T6G 2E1

[26] Erlangen Centre for Astroparticle Physics, Friedrich-Alexander-Universität Erlangen-Nürnberg, D-91058 Erlangen, Germany

[27] Technical University of Munich, TUM School of Natural Sciences, Department of Physics, D-85748 Garching bei München, Germany

[28] Département de physique nucléaire et corpusculaire, Université de Genève, CH-1211 Genève, Switzerland

[29] Dept. of Physics and Astronomy, University of Gent, B-9000 Gent, Belgium

[30] Dept. of Physics and Astronomy, University of California, Irvine, CA 92697, USA

[31] Karlsruhe Institute of Technology, Institute for Astroparticle Physics, D-76021 Karlsruhe, Germany

[32] Karlsruhe Institute of Technology, Institute of Experimental Particle Physics, D-76021 Karlsruhe, Germany

[33] Dept. of Physics, Engineering Physics, and Astronomy, Queen's University, Kingston, ON K7L 3N6, Canada

[34] Department of Physics & Astronomy, University of Nevada, Las Vegas, NV, 89154, USA

[35] Nevada Center for Astrophysics, University of Nevada, Las Vegas, NV 89154, USA

[36] Dept. of Physics and Astronomy, University of Kansas, Lawrence, KS 66045, USA

[37] Centre for Cosmology, Particle Physics and Phenomenology - CP3, Université catholique de Louvain, Louvain-la-Neuve, Belgium

[38] Department of Physics, Mercer University, Macon, GA 31207-0001, USA

[39] Dept. of Astronomy, University of Wisconsin–Madison, Madison, WI 53706, USA

[40] Dept. of Physics and Wisconsin IceCube Particle Astrophysics Center, University of Wisconsin–Madison, Madison, WI 53706, USA

[41] Institute of Physics, University of Mainz, Staudinger Weg 7, D-55099 Mainz, Germany

[42] Department of Physics, Marquette University, Milwaukee, WI, 53201, USA

[43] Institut für Kernphysik, Westfälische Wilhelms-Universität Münster, D-48149 Münster, Germany

[44] Bartol Research Institute and Dept. of Physics and Astronomy, University of Delaware, Newark, DE 19716, USA

[45] Dept. of Physics, Yale University, New Haven, CT 06520, USA

[46] Columbia Astrophysics and Nevis Laboratories, Columbia University, New York, NY 10027, USA

[47] Dept. of Physics, University of Oxford, Parks Road, Oxford OX1 3PU, United Kingdom

[48] Dipartimento di Fisica e Astronomia Galileo Galilei, Università Degli Studi di Padova, 35122 Padova PD, Italy

[49] Dept. of Physics, Drexel University, 3141 Chestnut Street, Philadelphia, PA 19104, USA

[50] Physics Department, South Dakota School of Mines and Technology, Rapid City, SD 57701, USA

[51] Dept. of Physics, University of Wisconsin, River Falls, WI 54022, USA

[52] Dept. of Physics and Astronomy, University of Rochester, Rochester, NY 14627, USA

[53] Department of Physics and Astronomy, University of Utah, Salt Lake City, UT 84112, USA

[54] Oskar Klein Centre and Dept. of Physics, Stockholm University, SE-10691 Stockholm, Sweden

[55] Dept. of Physics and Astronomy, Stony Brook University, Stony Brook, NY 11794-3800, USA

[56] Dept. of Physics, Sungkyunkwan University, Suwon 16419, Korea

[57] Institute of Physics, Academia Sinica, Taipei, 11529, Taiwan

[58] Dept. of Physics and Astronomy, University of Alabama, Tuscaloosa, AL 35487, USA

[59] Dept. of Astronomy and Astrophysics, Pennsylvania State University, University Park, PA 16802, USA

[60] Dept. of Physics, Pennsylvania State University, University Park, PA 16802, USA

[61] Dept. of Physics and Astronomy, Uppsala University, Box 516, S-75120 Uppsala, Sweden

[62] Dept. of Physics, University of Wuppertal, D-42119 Wuppertal, Germany

[63] Deutsches Elektronen-Synchrotron DESY, Platanenallee 6, 15738 Zeuthen, Germany

[64] Institute of Physics, Sachivalaya Marg, Sainik School Post, Bhubaneswar 751005, India

[65] Department of Space, Earth and Environment, Chalmers University of Technology, 412 96 Gothenburg, Sweden

[66] Earthquake Research Institute, University of Tokyo, Bunkyo, Tokyo 113-0032, Japan

Acknowledgements

11